2011 International Conference on Mechanical, Industrial, and Manufacturing Engineering
Lecture Notes in Information Technology Vols. 1-2

Stability of a Rotating Tank Source-Sink Setup to Model a Polar Vortex

Tony Vo and Gregory J. Sheard
Department of Mechanical and Aerospace Engineering
Monash University
Clayton, Victoria 3800, Australia
{Tony.Vo & Greg.Sheard}@monash.edu

Luca Montabone
Atmospheric, Oceanic and Planetary Physics
University of Oxford
Parks Road, Oxford OX1 3PU, United Kingdom
Montabone@atm.ox.ac.uk

The fundamental instabilities forming on a numerical rotating source-sink model is reported. The rotation of fluid combined with fluid injection from a source ring placed an appreciable distance away from the axis and the fluid withdrawal from a central sink generates a vortical structure similar to that seen in atmospheres.

Axisymmetric flow is computed on the meridional semi-plane using a spectral-element discretisation, and stability to non-axisymmetric perturbations is determined using a linear stability analysis. Direct numerical simulation (DNS) via a spectral element-Fourier method verifies the stability predictions. The solutions produce similar vortex structures to the experimental physics.

A global linear stability analysis predicts a structure with azimuthal wavenumber 13 arising from the flow which is higher than what was observed experimentally (wavenumbers of 1 to 6). Contour levels of the perturbation field indicate that perturbation structures are located at the source, rather than the sink, where laboratory dye visualization has been focused. Three-dimensional simulations suggest that these outer disturbances agitate lower-wavenumber instabilities near the axis (pole).

Index Terms – Polar vortex, Source-Sink, Numerical, Barotropic instabilities.

I. Introduction

Atmospheric vortices are abundant in nature and arise due to the ordinary rotation of the Earth. They are known for their coherent structures and the ability to harness great amounts of energy as seen in tornadoes. Distinct vortices, known as polar vortices have been observed to form at the polar regions on Earth. They are large in size and circular in shape. Polar vortices have been observed on planets with atmospheres, including Venus, Mars, Jupiter and Saturn, and their size, configuration and strength differs.

The combination of planetary rotation together with conservation of angular momentum causes circumpolar jets to develop at polar latitudes, which encircle the polar vortex. This structure can take on various geometric configurations, such as a dipole observed on Venus through to a hexagonal configuration, observed on Saturn by the Cassini spacecraft [3]. These configurations are not always stable and have demonstrated swift vacillation between states in over timescales in the order of days. A recent example was observed on Venus via the European Space Agency Venus Express probe where the southern structure transitioned between a dipole to a monopole, and back again over the span of a few Earth days, where one Venusian day equates to 243 Earth days [8].

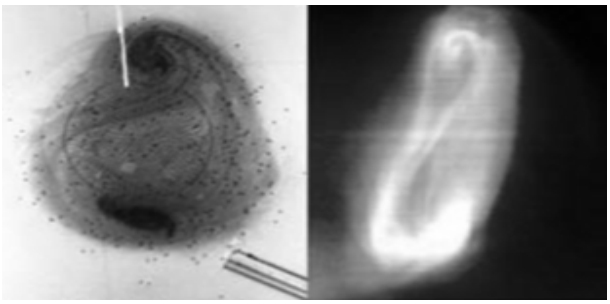

Fig. 1 An analogue between a mode-2 structure created in a laboratory (left) and its atmospheric counterpart (right). This figure is reproduced from [6]. The images represent a Venus dipole polar vortex.

Strong coherent vortices have the ability to trap particles in their cores and isolate them from the surrounding flow for extended periods [9]. This property poses issues for Earth's climate as polar vortices are prominent during winter, exacerbating chlorine build up. The onset of spring weakens and breaks up the polar vortex. This releases the chlorine which reacts with the ozone, depleting the ozone layer. Consequently, climate variability has been observed in the high-latitude Southern Hemisphere [13]. The effects propagate equatorward impacting countries such as Australia through prolonged drought conditions [7].

In pursuit of an understanding of the stability of polar vortices, models have recently been studied in the laboratory [6]. Vortex structures were generated which closely resembled the various configurations observed in the atmospheres. Fig. 1 depicts a comparison between a laboratory-produced vortex and a Venusian atmospheric polar vortex. A 5-metre diameter Coriolis tank in Trondheim, Norway, was used to produce model polar vortices with configurations featuring 1 to 6 repetitions around their circumference, which were observed via dye visualisation. The vortices were produced by rotating the cylindrical tank, and injecting fluid poleward from a source ring offset by extraction of fluid from a sink at the tank axis (the pole). Conservation of angular momentum increases the rotation rate of the poleward-moving fluid, thus generating the vortex near the axis. The injection and extraction of fluid also induces upwelling and downwelling effects, which are seen naturally in the Earth's atmosphere arising from temperature differences across latitudes. Thus the present source-sink method faithfully models several features of the polar atmospheric physics.

978-0-9831693-1-4/10/$25.00 ©2011 IERI

Given the complexity and current limited understanding of the dynamics involved in producing, stabilising and the vacillation of polar vortices, the immediate study is focused on the fundamental instabilities that form. As a result, the forcing parameters dictating the simulations in this preliminary study are lower than to those explored in [6].

II. Methodology

In this study the source-sink system in [6] will be numerically produced. A schematic representation of the apparatus is shown in Fig. 2. The polar vortex is generated by the rotation of the tank at angular velocity Ω, and the poleward flux flow from the source to sink.

The two determining factors for the stability of a polar vortex have been found to be most dependent on the Rossby number and the volume flux [6]. The Rossby number relates inertial forces to Coriolis forces, though in this configuration it is not a control parameter. Hence we instead define a Reynolds number given by

$$Re = \frac{{R_i}^2 \Omega}{\nu} \tag{1}$$

where R_i is the sink radius, and ν the kinematic viscosity of the working fluid. An experiment in [6] utilised water with one tank revolution per minute which equates to $Re \sim 21{,}200$.

The axisymmetric mesh is shown in Fig. 3, which represents the *z-r* plane of the apparatus over which the flow is computed. The meridional semi-plane is discretised into a mesh of quadrilateral elements. The vertical dotted line denotes the axis of rotation and spatial symmetry.

To simulate and invoke the appropriate dynamics acquired in the laboratory, certain boundary conditions have been applied. The bottom and side walls rotate at a rate of Ω, while the top boundary acts as a stress-free surface. The inlet and outlet vertical velocity for the source and sink are parabolic in profile, peaking at their radial centreline and relatively stationary at their edges. The curvature of the sink accounts for the β-effect at the planet's pole [5].

The working fluid is assumed to be incompressible and Newtonian. The flow is described by the Navier-Stokes equations

$$\frac{\partial \mathbf{u}}{\partial t} + (\mathbf{u} \cdot \nabla)\mathbf{u} = -\nabla P + \nu \nabla^2 \mathbf{u} \tag{2a}$$

$$\nabla \cdot \mathbf{u} = 0 \tag{2b}$$

where $\mathbf{u}$ is the velocity vector field and P is the kinematic pressure field. These equations are solved in cylindrical coordinates using an in-house code employing a spectral-element discretisation in space and a third-order time-integration scheme based on backward differentiation. The axisymmetric solver has been validated in studies [10, 11]. Within each macro element, Lagrangian tensor-product polynomial shape functions describe the flow: the polynomial degree can be varied to control spatial resolution. The polynomials are interpolated at the Gauss-Legendre-Lobatto quadrature points. This scheme is based on high-order splitting methods presented in [4].

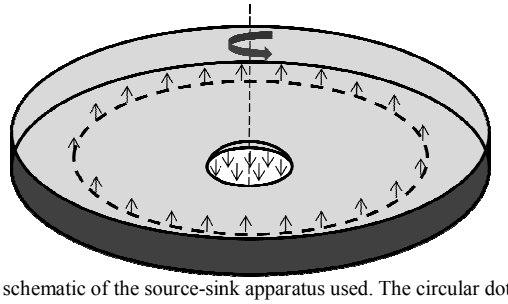

Fig. 2 A schematic of the source-sink apparatus used. The circular dotted line represents the source ring where fluid is injected and the vertical dotted line representing the axis of rotation. The arrows display flow direction.

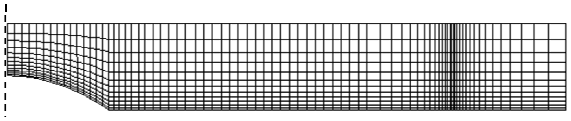

Fig. 3 Two-dimensional axisymmetric mesh of the *z-r* semi plane.

Our interest is in non-axisymmetric structures in the vortex flow and its stability, and thus a linear stability analysis is used to predict the fastest growing three-dimensional modes that develop on the underlying axisymmetric flow. An algorithm is executed which operates by computing the base flow and each of the perturbation fields separately. The saturated base flow is frozen and decoupled from the evolving three-dimensional perturbation fields. The eigenvalues of the system are obtained through a Floquet analysis [1]. Over sufficient periods of the flow solution, the leading eigenvalue is determined which corresponds to the Floquet multipliers μ of the system. The relationship between the Floquet multiplier and the growth rate σ is given by

$$\mu = e^{\sigma T} \tag{3}$$

where T denotes the time period. Thus, $|\mu| < 1$ represents a stable flow and $|\mu| > 1$ an unstable flow - the respective growth rates being positive and negative. The present implementation in cylindrical coordinates follows [12], and was recently validated in [2].

Focusing on the fundamental stability of the system, simulations have been performed for controlling parameters at lower values than those employed in [6]. Table I summarises the parameters used here and in an experiment from [6] as a comparison, as functions of *Re* and a poleward flux parameter

$$\bar{Q} = \frac{Q}{2\pi\Omega {R_o}^2 H}, \tag{4}$$

where Q denotes the injected/extracted fluid flow rate, R_o the radial distance from the axis to the source centreline and H representing the tank height.

TABLE I

Tabulated case studies and an experiment from Montabone *et al.* (2009) as defined by *Re* and $\bar{Q}$.

Case	*Re*	$\bar{Q}$ (10^{-4})
1	1325	3.04
2	4639	3.32
3	7952	3.61
4	11266	3.89
Laboratory	21206	4.75

III. Results

A. Axisymmetric Flow

Steady state solutions were obtained on the meridional semi-plane for the four flow cases. Fig. 4 represents the typical velocity fields exhibited by the flow in its steady state condition, via contours of vertical (axial) and radial velocity. It is apparent that the dominant dynamics occur in the boundary layer on the bottom boundary, known as the Ekman layer, and in the vicinity of the source and sink.

From [5], the measured relative azimuthal velocity profile (the local azimuthal velocity relative to the rotation of the tank) was observed to scale directly with r for regions between the axis and the sink's outer radius, and scales with $1/r$ thereafter. Azimuthal velocity data along the surface of the flow is presented in Fig. 5. A general trend of increasing peak velocities with increased Re and $\bar{Q}$ is demonstrated. The profile is qualitatively consistent with laboratory results. These profiles were found to be independent of height outside of the Ekman layer above the sink, verifying that the flow is strongly barotropic and that the setup reproduces the experimental physics. The peak location of the azimuthal velocity differed between the numerical and experimental results, with the latter peak closer to the sink edge. Further investigation has determined that to obtain the relative azimuthal velocity profile seen in the laboratory, the bulk of the sink outflow must have occurred near to the radial edge of the sink.

B. Linear Stability Analysis

Stability analysis was computed on each saturated axisymmetric base flow, and perturbations with azimuthal wavenumbers ranging from 1 to 20 were investigated. The global instability growth rates are shown in Fig. 6. The wavenumber is defined as $k = 2\pi/\lambda$ where λ is the azimuthal wavelength in radian. In each case the growth rate reaches a peak at a particular wavenumber before decreasing again at higher wavenumbers. The Re = 1325 case is found to be completely stable, with $k = 7$ the dominant wavenumber. This peak growth rate wavenumber correspondence increases with increasing Re and $\bar{Q}$.

Fig. 4 Contours of vertical (top) and radial (bottom) velocity depicting dynamic locality and boundary layers respectively for Re = 11266. Greyscale contours are used where light and dark shadings denote positive and negative values respectively.

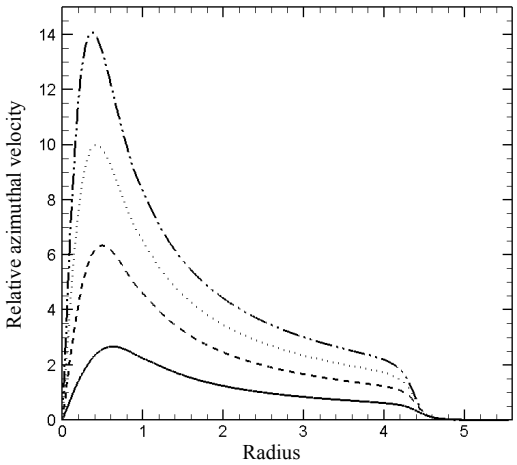

Fig. 5 Plots of the relative azimuthal velocity against normalized radius extracted from the surface of the flow for Re = 1325 (solid), Re = 4639 (dashed), Re = 7952 (dotted) and Re = 11266 (dash-dot-dot).

The case simulated with parameters most closely matching the laboratory conditions predicts a dominant instability mode with azimuthal wavenumber k = 13. This is higher than the wavenumbers observed in polar vortices and their laboratory models. A point of note is that the analysis is global and peak wavenumbers reflect modes across the entire flow. These do not necessarily correlate with the stability of the polar vortex region in isolation.

In the laboratory, visualization has been confined to the sink region near the axis, whereas stability analysis has predicted perturbation structures to be strongest in the vicinity of the source ring, as illustrated in Fig. 7.

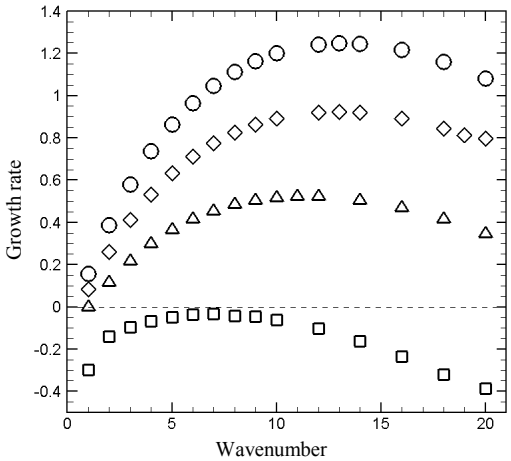

Fig. 6 Plots of growth rate against wavenumber obtained via linear stability analysis for Re = 1325 (square), Re = 4639 (triangle), Re = 7952 (diamond) and Re = 11266 (circle). The growth rates are non-dimensional and their values are deduced from the global domain.

Fig. 7 Perturbation contours of vertical vorticity displaying strong growth around the source radius for $Re = 4639$, $k = 13$. Greyscale contours are used where light and dark shadings denote positive and negative values respectively.

C. *Three-dimensional DNS*

Three-dimensional DNS computed over 16 Fourier mode expansions yield evolution of the predicted instability modes and are comparative to polar vortex configurations. The location of the prevailing instabilities agrees well with the linear stability results. Low-wavenumber disturbances have been observed near the sink.

Perturbation vorticity contours at the fluid surface are shown in Fig. 8, depicting an inner coherent structure with wavenumber 2. This structure has been seen to vacillate between a mode-1 and mode-2 configuration respectively representative of a circular and dipole structure in the atmosphere. The outer high-wavenumber disturbances developing around the source ring are unstructured and appear to act as a forcing perturbation that incites low-wavenumber instability structures to emerge near the sink. Regular patterns have been observed around the source under different forcing conditions. In such cases, the polar vortex remains to exhibit a low-wavenumber configuration. Global stability analysis did not detect structures forming near the axis, thus suggesting that stability analysis should be confined to the sink region.

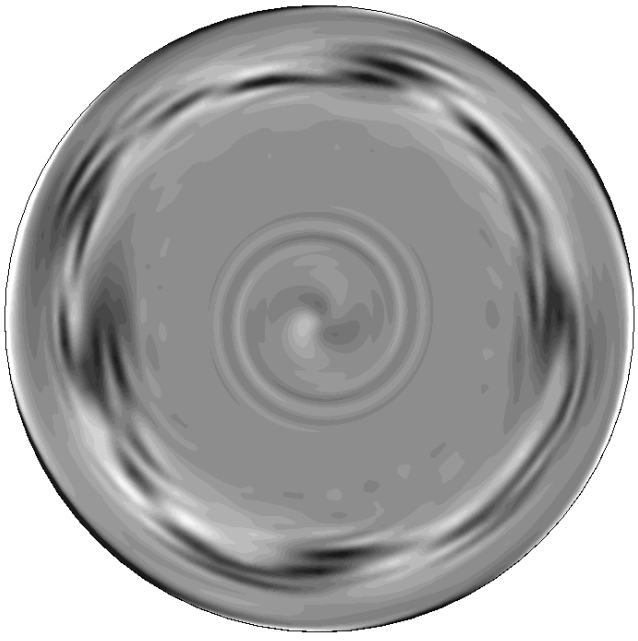

Fig. 8 A plan view of the surface where contours of vertical vorticity are shown. Greyscale contours are used where light and dark shadings denote positive and negative values respectively.

III. Conclusion

The fundamental instabilities occurring in polar vortices produced via a source-sink configuration have been numerically investigated. A computational mesh set up to emulate the dynamics of an experimental study [6], is the basis of this study. Base flow solutions indicate major dynamics taking place in the Ekman layer, source and sink locality.

Montabone *et al.* (2009) observed through dye visualisation, the polar vortex forming around the sink. Stability analysis dictates major growth appearing around the source ring which is visible in 3D DNS, although a polar vortex in the centre was also observed. This implies stability analysis should be performed on a truncated domain enclosing only the sink, in order to obtain growth rates that are reflective of the polar vortex.

Acknowledgments

T.V. received support through an Engineering Research Living Allowance and acknowledges the Monash University E-research centre for the access to its high performance computing facility, Sun Grid. Computations were also carried out with the support of a grant under the NCI Merit Allocation Scheme. NCI is supported by the Australian Commonwealth Government. G.J.S. is supported by a Faculty of Engineering Small Grant.

References

[1] D. Barkley, R. D. Henderson, "Three-dimensional Floquet stability analysis of the wake of a circular cylinder," Journal of Fluid Mechanics., 1996, vol. 322, pp. 215-241.

[2] S. J. Cogan, K. Ryan, G. J. Sheard, "Symmetry breaking and instability mechanisms in medium depth torsionally driven open cylinder flows," Journal of Fluid Mechanics, 2011, In Press.

[3] L. N. Fletcher, *et al*., "Temperature and composition of Saturn's polar hot spots and hexagon," Science, 2008, vol. 319, pp. 79-81.

[4] G. E. Karniadakis, M. Israeli and S. A. Orszag, "High-order splitting methods for the incompressible Navier-Stokes equations," J. Comput. Phys., 1991, vol. 97, no. 2, pp. 414-443.

[5] L. Montabone, *et al.*, "Barotropic instability of planetary polar vortices: CIV analysis of specific multi-lobed structures," Proceedings of the HYDRALAB III Joint User Meeting, Hannover, February 2010.

[6] L. Montabone, *et al.*, "Coherent Structures in Planetary Polar Vortices: A Laboratory View," International Conference on Comparative Planetology: Venus – Earth – Mars, ESTEC, Noordwijk, Netherlands, 11-15 May, 2009.

[7] B. F. Murphy and B. Timbal, "A review of recent climate variability and climate change in southeastern Australia," International Journal of Climatology, 2008, vol. 28, pp. 859-879.

[8] G. Piccioni, *et al.*, "South-polar features on Venus similar to those near the north pole," Nature, 2007, vol. 450, pp. 637-640.

[9] A. Provenzale, "Transport by coherent barotropic vortices," Annu. Rev. Fluid Mech., 1999, vol. 31, pp. 55-93.

[10] G. J. Sheard, "Flow dynamics and wall shear stress variation in a fusiform aneurysm," Journal of Engineering Mathematics, 2009, vol. 64, no. 4, pp. 379-390.

[11] G. J. Sheard and K. Ryan, "Pressure-driven flow past spheres moving in a circular tube," Journal of Fluid Mechanics, 2007, vol. 592, pp. 233-262.

[12] G. J. Sheard, M. C. Thompson and K. Hourigan, "The subharmonic mechanism of the Mode C instability," Physics of Fluids, 2005, vol. 17, no. 11, article no. 111702.

[13] D. W. J. Thompson and S. Solomon, "Interpretation of recent Southern Hemisphere climate change," Science, 2002, vol. 296, pp. 895-899.